Nanoscale Advances

ROYAL SOCIETY OF CHEMISTRY

PAPER

View Article Online
View Journal | View Issue

Cite this: *Nanoscale Adv.*, 2025, **7**, 1326

Microwave-assisted synthesis of highly photoluminescent core/shell CuInZnSe/ZnS quantum dots as photovoltaic absorbers†

Shubham Shishodia,[ab] Hervé Rinnert,[b] Lavinia Balan,[c] Jordane Jasniewski,[d] Stéphanie Bruyère,[b] Ghouti Medjahdi,[b] Thomas Gries[b] and Raphaël Schneider *[a]

Received 29th October 2024
Accepted 7th January 2025

DOI: 10.1039/d4na00893f

rsc.li/nanoscale-advances

Water-dispersible core/shell CuInZnSe/ZnS (CIZSe/ZnS) quantum dots (QDs) were efficiently synthesized under microwave irradiation using *N*-acetylcysteine (NAC) and sodium citrate as capping agents. The photoluminescence (PL) emission of CIZSe/ZnS QDs can be tuned from 593 to 733 nm with varying the Zn : Cu molar ratio in the CIZSe core. CIZSe/ZnS QDs prepared with a Zn : Cu ratio of 0.5 exhibit the highest PL quantum yield (54%) and the longest PL lifetime (515 ns) originating from the recombination of donor–acceptor pairs. The potential of CIZSe/ZnS QDs as photoabsorbers in QD-sensitized solar cells was also evaluated. An adequate type-II band alignment is observed between TiO_2 and CIZSe/ZnS QDs, indicating that photogenerated electrons in CIZSe/ZnS QDs could efficiently be injected into TiO_2.

Introduction

Over the past three decades, binary group II–VI semiconductor nanocrystals (quantum dots, QDs) with a relatively narrow bandgap, such as CdSe or CdTe, have been extensively studied due to their tunable and narrow photoluminescence (PL) emission, high PL quantum yield (PL QY) and high photostability.[1,2] However, their practical applications are limited due to the toxicity concern of Cd and the associated environmental issues.[3] Recently, many efforts have been made to prepare eco-friendly QDs with PL characteristics comparable to Cd-based ones.

I–III–VI_2 QDs, like $AgInS_2$ or $CuInS_2$, and their quaternary derivatives AgInZnS or CuInZnS obtained after shelling and alloying with ZnS, have been demonstrated to be excellent alternatives to II–VI QDs for numerous applications including QD-sensitized solar cells (QDSSCs), fluorescence bio-imaging and light-emitting diodes.[4–7] I–III–VI_2 QDs exhibit a narrow bandgap, high absorption coefficients, a broad light absorption ranging from the UV to the NIR and a high thermal stability, conditions required for any use of these nanocrystals in technologies related to the conversion of solar energy.[7–9] Moreover, I–III–VI_2 QDs exhibit a high tolerance to stoichiometric deviation and defects, allowing a composition-dependent band structure which can be used in particular when coupling with other semiconductors to promote the transport and the separation of charge carriers.[10–13]

Recently, $CuInSe_2$ (CISe) QDs have attracted high interest for photovoltaic applications due to their small bandgap (1.04 eV), high light absorption coefficient (*ca.* 10^5 cm^{-1}) and large Bohr exciton radius (10.6 nm).[8,14–16] Hydrophobic CISe core QDs and core/shell CISe/ZnS QDs capped with oleylamine, dodecanethiol or oleic acid can be prepared by thermal decomposition of metal precursors and Se in a high boiling point solvent like 1-octadecene followed by the deposition of the ZnS shell.[16–21] These nanocrystals can also be synthesized by the hot injection of a Se precursor into a mixture of metal precursors.[22–33] The optical properties of the QDs are excellent with optical absorption covering the entire visible and near IR range and PL QYs up to almost 100%.[33] However, the use of these oil-dispersible nanocrystals in QDSSCs requires an additional ligand exchange step, for example with 3-mercaptopropionic acid (3-MPA), in order to make them hydrophilic and allow their anchoring onto TiO_2 films.

An alternative is the preparation of CIZSe core QDs in an aqueous medium. The synthesis processes in an aqueous medium use fewer toxic precursors and ligands than those necessary for synthesis in an organic medium and the reaction conditions are generally milder. However, the preparation of CIZSe and CIZSe/ZnS QDs in an aqueous medium has been significantly less studied than in organic media. Syntheses are most commonly performed at reflux or under microwave activation using a mixture of glutathione (GSH) and sodium citrate as ligands.[34–37] The use of gelatin and thioglycolic acid (TGA) or

[a]*Université de Lorraine, CNRS, LRGP, F-54000 Nancy, France. E-mail: raphael.schneider@univ-lorraine.fr*

[b]*Université de Lorraine, CNRS, IJL, F-54000 Nancy, France*

[c]*CEMHTI-UPR 3079 CNRS, Site Haute Température, 1D avenue de la Recherche Scientifique, 45071 Orléans, France*

[d]*Université de Lorraine, LIBio, F-54000 Nancy, France*

† Electronic supplementary information (ESI) available: UV-visible and PL emission spectra, FT-IR spectra, EDX analysis, TGA analysis, XPS spectra, ICP-OES analysis, TEM image and SAED pattern, PL quenching by TiO_2. See DOI: https://doi.org/10.1039/d4na00893f

of trithiocyanuric acid when the synthesis is carried out in an autoclave has also been reported.[38,39] The nanocrystals produced using these methods are of very small sizes (between 2 and 5.5 nm). Except the Mn^{2+}-doped CIZSe/ZnS QDs whose PL QY is 40%,[37] PL QYs are between 4 and 23.3%.

Herein, we report a microwave-assisted aqueous phase synthesis of core/shell CIZSe/ZnS QDs using *N*-acetylcysteine (NAC) and sodium citrate (SC) as capping ligands. By varying the Zn : Cu molar ratio from 5 to 0 in the CIZSe core, the PL emission can be tuned from the visible (593 nm) to the NIR (733 nm). Nanocrystals prepared with the Zn : Cu ratio of 0.5 exhibit the highest PL QY (54%) and the longest PL decay lifetime (515 ns). These nanocrystals exhibit a small diameter (2.2 ± 0.1 nm), indicating that the synthesis method developed allows a good size control. The potential of CIZSe/ZnS QDs as absorbers for photovoltaic cells was also investigated.

Results and discussion

Synthesis and optical properties of CIZSe/ZnS QDs

CIZSe core nanocrystals were prepared *via* a colloidal synthetic method under microwave (MW) irradiation using $Cu(NO_3)_2$, $In(NO_3)_3$ and $Zn(NO_3)_2$ as metal precursors (Scheme 1). Note that Cu^{2+} cations will be reduced *in situ* to Cu^+ by Se^{2-} anions. To regulate the reactivities of Cu^+, In^{3+} and Zn^{2+} cations, a soft organic base (an organic thiol) was associated with the soft Lewis acid Cu^+ while the hard Lewis base sodium citrate was used to bind with the hard Lewis acid In^{3+}. With an intermediate hardness between those of In^{3+} and Cu^+, Zn^{2+} ions can bind to both sodium citrate and thiol. To tune the optical absorption and the PL emission relative to conventional CISe QDs, Zn^{2+} ions were doped in the CISe core and the Zn : Cu elemental ratio was varied while maintaining the amount of In.[36,40] In preliminary experiments not described in detail here, we varied the time and power of microwave irradiation, the sulfur ligand associated to sodium citrate and the pH of the reaction medium to optimize the PL intensity of CIZSe/ZnS QDs. These trials showed that two pulses of 180 W for 2.5 min for the CIZSe core and one of 180 W for 2 min for the shell deposition allow to obtain CIZSe/ZnS QDs with the strongest PL intensity. Among the studied thiol ligands (*N*-acetylcysteine, glutathione, 3-mercaptopropionic acid, 2-mercaptopropionic acid, mercaptosuccinic acid, dimercaptosuccinic acid, and thioglycolic acid), the best results were obtained using NAC (Fig. S1†). Finally, an adjustment of the pH of the reaction mixture to 6 before microwave heating allows to obtain the highest PL intensity (Fig. S2†).

In a typical CIZSe/ZnS QDs synthesis, the metal precursors ($Cu(NO_3)_2$, $In(NO_3)_3$ and $Zn(NO_3)_2$) and the ligands (NAC and sodium citrate) were dissolved in water and the pH adjusted to 6. Next, freshly prepared NaHSe was quickly injected under stirring and the mixture transferred into a MW oven for 5 min. After the core growth, a ZnS shell was deposited on the surface of CIZSe QDs by adding $Zn(NO_3)_2$, thiourea and NAC and further heating under MW irradiation for 2 min (Scheme 1).

The presence of Cu in the core is essential to observe a PL signal. Core CIZSe QDs exhibit a low PL intensity due to high density of surface and intrinsic defects like In substituted Cu (In_{Cu}), which cause non-radiative recombination of the photo-excited carrier (see Fig. S3† for QDs prepared with a Zn : Cu ratio of 0.5). The presence of the In_{Cu}-related absorption can be observed at *ca.* 1200 nm on UV-visible-near infrared diffuse reflectance spectra (Fig. S3†).[39] The PL QYs of CIZSe QDs are lower than 2%. However, after ZnS shelling, the PL QYs markedly increase, reaching values up to 54% for QDs prepared with a Zn : Cu ratio of 0.5 (*vide infra*), through the effective passivation of CIZSe QDs surface which allows to remove some surface-related non-radiative centers and thus improve the optical stability. A significant blue-shift from 722 to 685 nm of the PL peak position is observed after the ZnS shelling, indicating the further incorporation of Zn^{2+} cations into the CIZSe core, resulting in an increase in the bandgap energy (Fig. S4†).

CIZSe/ZnS QDs absorb over the whole visible region and even in the near infrared for QDs containing little or no Zn (Fig. 1a). No distinctive excitonic peak can be observed for CIZSe/ZnS QDs due to their heterogeneous composition distributions that generate a wide distribution of vibrational states (intrinsic and surface trap states), which is a typical feature of I–III–VI_2 QDs.[41–43] A gradual red-shift of the UV-visible band edge is observed when decreasing the Zn : Cu ratio, indicating a composition-dependent variation of the energy bandgap. Fig. 1b shows the plots of $(\alpha h\gamma)^2$ *vs.* $h\gamma$ (where α is the absorption coefficient and $h\nu$ is the photon energy) used to determine the energy bandgap of CIZSe/ZnS QDs. E_g values were obtained by extrapolating the linear portion of the curve to the intercept with the *x* axis and were found to be 1.73, 1.80, 1.88, 1.93, 1.98 and 2.12 eV for Zn : Cu ratios of 0, 0.2, 0.5, 1.0, 2.0 and 5.0, respectively.

As seen in Fig. 1c, the PL emission can be tuned from 593 to 733 nm when increasing the Cu content, is broad (full-width at half-maximum, fwhm, of *ca.* 125 nm) and shows a large Stokes shift. The broad PL emissions are associated to intragap surface states and intrinsic defect states involving donor–acceptor pairs (DAPs).[41–43] The sample prepared with a Zn : Cu ratio of 0.5 has the highest PL QY (54%) (Table 1). The PL QYs of other CIZSe/ZnS are between 21 and 33%. The excitation wavelength was tuned from 275 to 650 nm and the PL emission was found to vary as shown in the excitation-emission 3D map (Fig. 1d). The excitation-dependent PL likely originates from the different relaxations pathways previously mentioned. The highest PL emission intensity is observed at 644 nm when CIZSe/ZnS QDs are excited at 396 nm.

Scheme 1 Schematic representation of CIZSe and core/shell CIZSe/ZnS QDs synthesis.

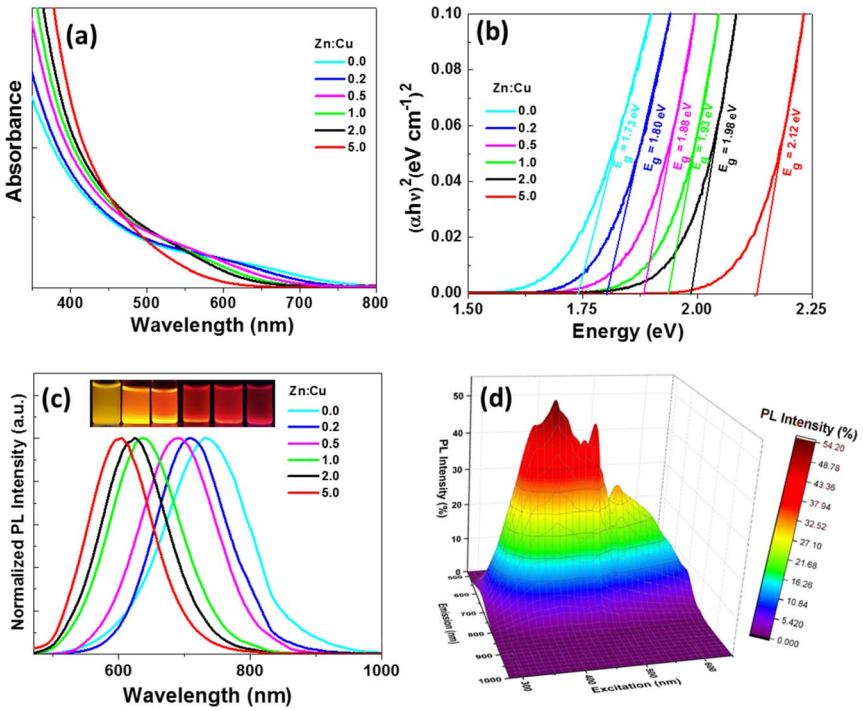

Fig. 1 (a) UV-visible absorption spectra, (b) Tauc plots used for the determination of the optical bandgap, (c) PL emission spectra after excitation at 450 nm of CIZSe/ZnS QDs when varying the Zn : Cu ratio (the inset is a digital photograph of aqueous dispersions of QDs under UV illumination). (d) PL excitation-emission 3D map of CIZSe/ZnS QDs prepared with a Zn : Cu molar ratio of 0.5.

Table 1 PL QYs and PL lifetime decays of core/shell CIZSe/ZnS QDs

Zn : Cu ratio	PL QY (%)	A_1	τ_1 (ns)	A_2	τ_2 (ns)	A_3	τ_3 (ns)	τ_{av} (ns)
0	21	0.128	210	0.0059	674	0.0004	7080	252
0.2	31	0.169	229	0.0086	801	0.0013	10 800	332
0.5	54	0.116	268	0.0007	1120	0.0027	10 800	515
1	33	0.072	277	0.0024	1210	0.0010	11 300	455
2	24	0.201	225	0.0079	899	0.0012	10 500	310
5	24	0.185	271	0.0217	948	0.0022	10 000	442

The PL emission wavelength can also be regulated through changing the precursor molar ratio of Cu : In or In : Se in the reaction. When increasing the Cu : In molar ratio, the PL emission of CIZSe/ZnS QDs was found to shift to long-wavelength region due to the bandgap narrowing (Fig. S5†).[44] With the increase of the Se content in CIZSe/ZnS nanocrystals, the PL emission shifts to shorter wavelengths, indicating an increase of the bandgap (Fig. S6†). Besides, all CIZSe and CIZSe/ZnS QDs show a broad absorption from 250 to 650 nm.

The photostability of a colloidal dispersion of CIZSe/ZnS QDs (Zn : Cu = 0.5) was also compared to that of Rhodamine B (RhB) under continuous irradiation of a Hg/Xe lamp (light irradiance of 50 mW cm^{-2}), at 20 °C and under ambient conditions (Fig. S7†). A decrease in PL intensity of CIZSe/ZnS QDs (Zn : Cu = 0.5) of about 17% is observed after 90 min of irradiation before reaching a quasi-plateau after 240 min irradiation. This decrease likely originates from a photo-oxidation of QDs during the irradiation. Noteworthy is also that the fwhm of the PL signal is almost constant and that no additional PL signals related to defects could be observed. For RhB, the decrease in PL intensity is faster and regular throughout the irradiation and only 40% of the initial intensity is maintained after 240 min irradiation, indicating that CIZSe/ZnS QDs are more photostable than a conventional organic dye like RhB.

The PL emission mechanism of CIZSe/ZnS QDs was investigated by measuring their PL lifetime (Fig. 2a). The normalized PL decay curves were fitted by a tri-exponential function:

$$I(t) = A_1 \exp(-t/\tau_1) + A_2 \exp(-t/\tau_2) + A_3 \exp(-t/\tau_3)$$

where τ_1, τ_2 and τ_3 are the lifetimes and A_1, A_2 and A_3 the coefficients of fitting parameters, respectively. The results are listed in Table 1. The evolution of τ_1, τ_2 and τ_3 values when varying the Zn : Cu molar ratio is shown in Fig. 2b. As can be seen, the short PL lifetime τ_1 is only weakly influenced by the Zn content of the nanocrystals and is likely related to non-radiative processes as previously described.[32,41–43] The highest PL QYs are measured for samples prepared with Zn : Cu ratios of 0.2, 0.5 and 1, which correspond to CIZSe/ZnS QDs exhibiting the highest medium (τ_2) and longest (τ_3) decays. These decays correspond to radiative processes dependent on surface defect states and DAPs. Regarding the Zn : Cu ratio, τ_2, and to a lesser extent τ_3, increase with the Zn : Cu ratio from 0 to 1, indicating a promotion of energy transfer processes. As a result, the average PL lifetimes τ_{av} increases up to 515 ns for CIZSe/ZnS QDs prepared with a Zn : Cu ratio of 0.5. By further increasing the Zn : Cu ratio (2 or 5), a weak decrease of τ_2 and τ_3 values is

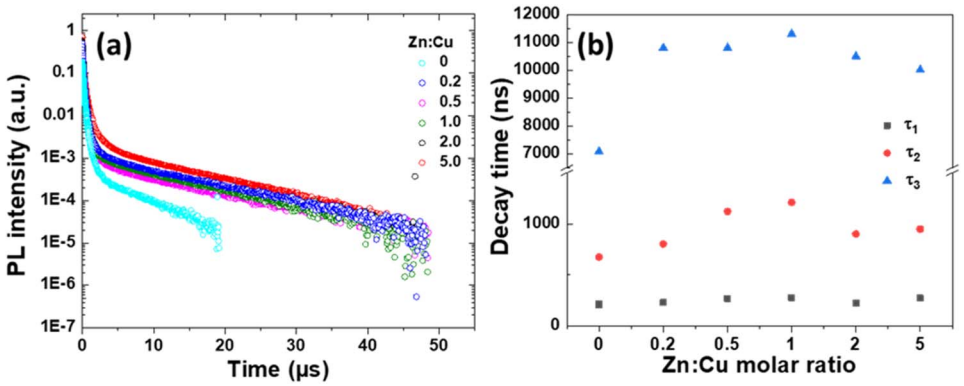

Fig. 2 (a) PL decay traces of CIZSe/ZnS QDs when varying the Zn : Cu molar ratio. PL decays were recorded at the PL maximum wavelength after excitation at 450 nm. (b) Evolution of τ_1, τ_2 and τ_3 decay times when varying the Zn : Cu molar ratio.

observed. The high PL QY determined for the sample prepared with a Zn : Cu ratio of 0.5 likely results from the low contribution of non-radiative processes combined to the large weight of radiative processes involved in the PL emission. The average PL lifetimes determined for CIZSe/ZnS QDs are significantly higher than those of CISe/ZnS QDs prepared in aqueous phase (*ca.* 150–250 ns)[35,36,39] and are similar to those of CISe/ZnS QDs prepared in organic phase,[18] suggesting that the synthesis method developed in this work (incorporation of Zn^{2+} ions in the CISe core before depositing the ZnS shell and microwave heating) allows to restrain nonradiative processes.

Structural characterizations

The crystalline structure of core/shell CIZSe/ZnS QDs was first assessed by XRD. The XRD patterns show that CIZSe/ZnS QDs exhibit the chalcopyrite tetragonal structure as indicated by (112), (204)/(220) and (312)/(116) reflections (JCPDS No. 01-087-2265), which agrees well with literature.[45] The broadness of XRD signals also confirms the nanocrystalline nature of the samples. With the increasing Zn^{2+} content, the XRD signals slightly shift to higher angles due to the lattice contraction originating from the incorporation of higher amounts of Zn^{2+} ions with a smaller ion radius (0.6 nm) than that of In^{3+} (0.62 nm). CIZSe/ZnS QDs prepared with Zn : Cu molar ratios of 0, 0.2, 0.5 and 1.0 show a pure tetragonal phase. However, cubic $In(OH)_3$ (JCPDS No. 04-008-9898) was detected for QDs prepared with the highest Zn : Cu ratios (2.0 and 5.0). The formation of $In(OH)_3$ likely originates from the $In^{3+} \rightarrow Zn^{2+}$ cation exchange either during the core growth and/or the ZnS shelling followed by the reaction of In^{3+} cations with hydroxide anions present in the reaction medium. The presence of $In(OH)_3$ was confirmed by TEM (Fig. S8a†) and the associated SAED pattern (Fig. S8b†) which shows the co-existence of CIZSe/ZnS and $In(OH)_3$ nanocrystals in samples prepared with Zn : Cu ratios of 2.0 and 5.0.

Dynamic light scattering (DLS) measurements conducted on NAC-capped CIZSe/ZnS QDs prepared with a Zn : Cu ratio of 0.5 and selected as representative are shown in Fig. 3b. The volume-weighted size distribution shows that the sample is composed of very small QDs with an average size of *ca.* 2 nm and that the colloidal dispersion is almost monodisperse (PDI = 0.2). The intensity-weighted distribution seems to indicate that the sample is more heterogeneous but this analysis gives a much greater weight to nanoparticles of larger size which only represent a very small fraction of the sample.

The carboxylate group of NAC provides to CIZSe/ZnS QDs a zeta (ζ) potential of −47 mV at pH = 7 (Fig. 3c). This highly negative ζ potential will not only influence the colloidal stability of the dots in aqueous media but also their optical properties such as recombination dynamics.[46]

The diameter of CIZSe/ZnS QDs was determined using HAADF-STEM and TEM (Fig. 4a and b). Quasi-spherical nanoparticles with an average diameter of 2.2 ± 0.1 nm can be observed (inset of Fig. 4b). The lattice spacing of 0.33 nm measured on the HR-TEM image can be indexed to the (112) plane of $CuInSe_2$. The HR-TEM image and the associated selected area electron diffraction (SAED) pattern confirm the high crystallinity of CIZSe/ZnS QDs (Fig. 4c and d). No interface can be seen between the CIZSe core and the ZnS shell likely due to the thin layer of ZnS covering the CIZSe core and/or the

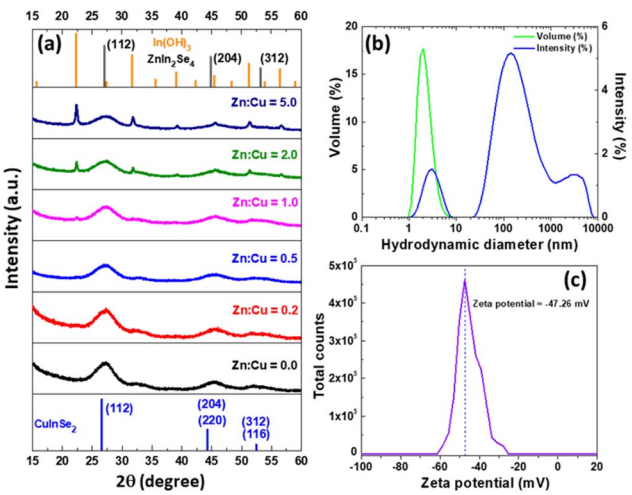

Fig. 3 (a) XRD patterns of CIZSe/ZnS QDs. (b) Hydrodynamic diameter and (c) ζ potential of CIZSe/ZnS QDs prepared with a Zn : Cu ratio of 0.5.

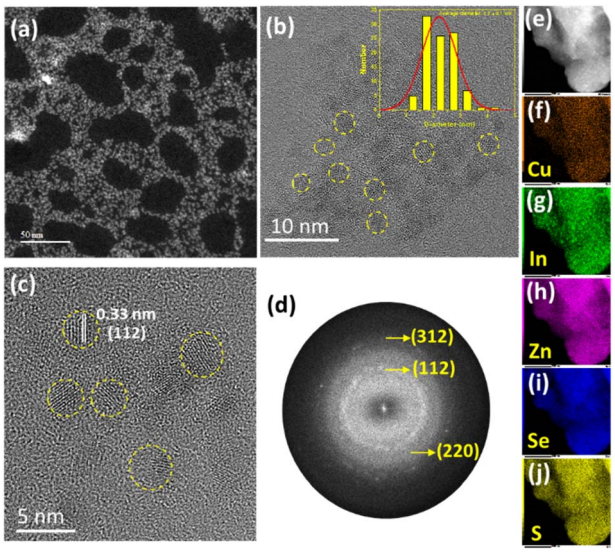

Fig. 4 (a) HAADF-STEM and (b) TEM images of CIZSe/ZnS QDs (the inset of (b) is the size distribution). (c) HR-TEM image of CIZSe/ZnS QDs and (d) the associated SAED pattern. (e–j) EDX elemental mapping.

alloying of ZnS with the core. The EDS analysis and the associated elemental confirm the presence of Cu, In, Zn, S and Se elements as well as their homogenous distribution in CIZSe/ZnS QDs (Fig. 4e–j and S9†).

The presence of NAC at the surface of QDs was confirmed by FT-IR (Fig. S10†). The signals observed at 3374, 2574 and 1718 cm^{-1} for NAC correspond to N–H, S–H and C=O stretchings, respectively. Compared to NAC, all QDs exhibit a broad signal at *ca.* 3300 cm^{-1} corresponding to the O–H stretching of the carboxylic acid group and/or to chemisorbed water molecules. The peaks with the highest intensity at *ca.* 1585 and 1380 cm^{-1} can be assigned to the asymmetric and symmetric stretching modes of the carboxylate function, respectively. This high density of carboxylate functions at the surface of QDs allows QDs to be dispersible in aqueous media and of high colloidal stability, which agrees with ζ potential measurements. Fig. S11† plots the thermogravimetric analyses from room temperature to 800 °C of CIZSe/ZnS QDs. A first weight loss of *ca.* 7% is observed between 30 and 150 °C and likely corresponds to the removal of chemisorbed water molecules and of neutral ligands (L-ligands) from the QDs surface. A second weight loss of *ca.* 20% originating from the decomposition of organic ligands ionically bound (X-ligands) to the QDs surface occurs between 250 and 450 °C.[47] These results show that ligands participate in *ca.* 25% of the mass of QDs.

XPS was further used to determine the chemical composition as well as the bonding state of elements composing CIZSe/ZnS QDs. The XPS survey spectrum of CIZSe/ZnS QDs prepared with a Zn : Cu ratio of 0.5 indicates that Cu, In, Zn, Se, S, C, N, O and Na are present and that no other elements are detected, indicating the purity of the nanocrystals (Fig. S12†). C, N, O and Na elements correspond to the capping ligands (NAC and sodium citrate) of CIZSe/ZnS QDs. The HR XPS spectrum of Cu $2p_{3/2}$ shows a single signal at 932.08 eV corresponding to Cu in the +1 oxidation state in $CuInSe_2$,[30,32] confirming that the Cu^{2+} precursor is reduced into Cu^{+} during the synthesis (Fig. S13a†). The In $3d_{5/2}$ peaks at 444.34 and 451.86 eV are indicative of In(+3) (Fig. S13b†) while the Zn $2p_{3/2}$ signal at 1021.40 eV corresponds to Zn(+2) (Fig. S13c†).[30,32] The signals of Se $3d_{5/2}$ appear at 53.61 and 54.46 eV and show the presence of Se(−2) (Fig. S13d and e†). The presence of two signals suggest that Se(−2) is involved in different bonds with In^{3+}, Cu^{+} and Zn^{2+}. The S 2p core level spectrum shows two signals at 161.70 and 162.90 eV, corresponding to Cu–S and In–S bonds, respectively (Fig. S13d†).[48] The quantification of XPS signals indicates that the Cu/In/Zn ratio is of *ca.* 1/7.9/24.2 while the theoretical ratio is of 1/10/85. ICP-OES analyses carried out on CIZSe/ZnS QDs after purification show that the percentages in In and especially in Zn are lower than theoretical values (Table S1†). This deviation suggests that the Cu precursor reacts faster than In and Zn ones with Se^{2-} in the reaction medium.

Finally, XRD, TEM, FT-IR and XPS analyses further confirm that CIZSe/ZnS QDs were successfully prepared by the microwave-assisted hydrothermal method developed in this work.

Photoelectrochemical properties

In a first step, the flat band potentials of TiO_2 and CIZSe/ZnS QDs were determined using Mott–Schottky plots recorded after QDs deposition on FTO by dip-coating (Fig. 5a–g). The flat band potential V_{FB} was obtained by extrapolation of the linear part of the Mott–Schottky plots. For CIZSe/ZnS QDs prepared with Zn : Cu molar ratios of 0, 0.2, 0.5, 1, 2 and 5, V_{FB} values were determined to be of −0.32, −0.33, −0.34, −0.53, −0.55 and −0.61 V *vs.* NHE, respectively, while the V_{FB} value for TiO_2 is −0.26 V. The positive slopes of Mott–Schottky plots indicate that all CIZSe/ZnS QDs are n-type semiconductors. For this type of semiconductor, the conduction band (CB) edge is located at a slightly lower potential (*ca.* 0.1 V) with respect to its V_{FB}.[49] The position of the valence band (VB) of these QDs was determined using the energy bandgap estimated using the Tauc plots (Fig. 1b) and the results are described in Fig. 5h. The position of the valence band is only slightly impacted by the Zn : Cu ratio and varies between +1.30 to +1.44 V. On the other hand, when the Zn : Cu ratio increases from 0 to 5, the position of the conduction band is moved towards increasingly negative values (from −0.42 to −0.71 eV). This phenomenon is directly related to the increase in bandgap energy with the increase in Zn content in the CIZSe cores.

In QDSSCs, QDs anchored on the TiO_2 photoanode act as light absorbers. Upon photoexcitation, electrons are injected from the QD excited state into the conduction band of the TiO_2 layer that provides a fast channel for these electrons to transfer to the external circuit. Thus, engineering photoanodes of high stability and with high electrical conductivity is of high importance for enhancing the photoelectric conversion efficiency.[50] As the electron injection rate from QDs into the conduction band of TiO_2 plays a key role on photovoltaic

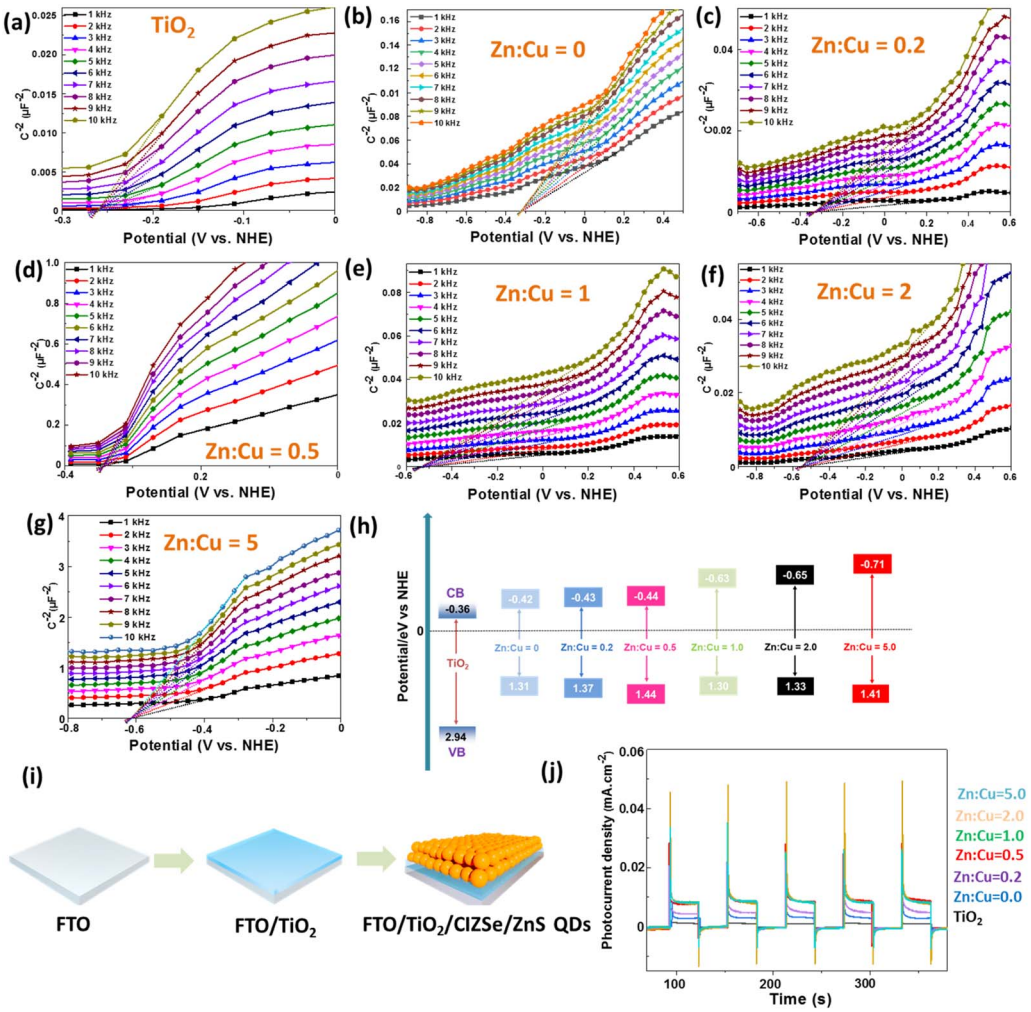

Fig. 5 (a–g) Mott–Schottky curves of TiO_2 thin film and of CIZSe/ZnS QDs (Zn : Cu = 0, 0.2, 0.5, 1, 2 and 5) deposited on FTO. (h) Electronic band structure of TiO_2 and CIZSe/ZnS QDs determined using flat band potentials and bandgap energies, (i) preparation of the FTO/TiO_2/CIZSe/ZnS photoelectrode, (j) transient photocurrents recorded for TiO_2 and TiO_2/CIZSe/ZnS layers on FTO (125 nm TiO_2 layer thickness, AM 1.5 G filter).

performance, the interaction of CIZSe/ZnS QDs (Zn : Cu = 5.0) with a TiO_2 colloid was investigated by PL.[51] As can be seen on Fig. S14a,† the addition of 50 μL of a TiO_2 colloid to 3 mL of an aqueous dispersion of CIZSe/ZnS QDs leads to an immediate decrease of a factor two of the PL intensity, indicating that QDs strongly bind to TiO_2 nanoparticles and that photo-excited electrons in QDs efficiently transfer to TiO_2. The decrease in PL intensity is not linear and is less pronounced after adding a larger amount of the TiO_2 colloid (up to 550 μL) (Fig. S14b†).

As previously shown, a suitable type II band alignment is observed for all CIZSe/ZnS QDs and TiO_2, which should favor the charge transfer from QDs to TiO_2.[52] This has been demonstrated by deposition of a TiO_2 layer with a thickness of *ca.* 125 nm onto FTO by magnetron sputtering followed by CIZSe/ZnS QDs *via* dip coating (Fig. 5i). The transient photocurrent responses of the TiO_2/CIZSe/ZnS samples prepared with Zn : Cu ratios of 5.0, 2.0, 1.0 and 0.5 are about six times higher than that of TiO_2, which confirms the improved carriers separation and transfer (Fig. 5j).

Conclusions

In summary, a fast and green synthetic route to prepare high quality water dispersible CIZSe/ZnS QDs was developed. CIZSe/ZnS QDs of small size (*ca.* 2.2 nm) and with excellent optical properties (PL QY up to 54% and PL lifetime up to 515 ns) were produced. The use of CIZSe/ZnS QDs as light absorbers for QDSSCs was explored. An adequate band alignment of QDs relative to TiO_2 was demonstrated for all QDs prepared indicating that photogenerated electrons in QDs can effectively transfer to TiO_2 and increase the photocurrent of the electrode. Future work will include the improvement of the device performance.

Experimental section

Chemicals

$In(NO_3)_3$ hydrate (99.99%, Thermo Fisher Scientific), $Cu(NO_3)_2 \cdot 3H_2O$ (99%, Merck), $Zn(NO_3)_2 \cdot 6H_2O$ (99%, Thermo Fisher Scientific), trisodium citrate dihydrate (99%, Thermo

Fisher Scientific), *N*-acetyl-L-cysteine (>98%, Thermo Fisher Scientific), SeO_2 (99.999%, Thermo Fisher Scientific), $NaBH_4$ (99%, Merck), thiourea CH_4N_2S (99+%, Thermo Fisher Scientific) and NaOH (VWR Chemicals) were used as received. Deionized Milli-Q water was used as solvent.

Synthesis of Cu–In–Zn–Se (CIZSe) core QDs

Typically, for the synthesis of CIZSe QDs with Zn : Cu molar ratio of 0.5 as an example, $In(NO_3)_3 \cdot 5H_2O$ (0.20 mmol), $Cu(NO_3)_2 \cdot 3H_2O$ (0.04 mmol), $Zn(NO_3)_2 \cdot 6H_2O$ (0.02 mmol), trisodium citrate dihydrate (0.34 mmol), and *N*-acetyl-L-cysteine (0.243 mmol) were dissolved into 30 mL of Milli-Q water in a 50 mL three-necked flask. The pH of the resultant mixture was adjusted to 6 by adding dropwise a 2 M NaOH solution under stirring. Separately, the selenium precursor was prepared at room temperature by adding SeO_2 (1 mmol) and $NaBH_4$ (2 mmol) into 5 mL of Milli-Q water, which was then reacted for 10 min under strong magnetic stirring and nitrogen protection to form a transparent NaHSe precursor solution. Then, 1.6 mL of the NaHSe solution was added into the three necked flask containing optically clear solution of nitrate salts and ligands under intermediate magnetic stirring and nitrogen purging, which turned reddish-brown instantaneously. Next, the reddish-brown mixture was kept under constant stirring and nitrogen protection for 15 minutes before being transferred to a Teflon-sealed microwave reactor. The microwave reactor was heated in a microwave oven at 180 W for two brief pulses of 2.5 min each with an interval of 1 min in between to form Cu–In–Zn–Se core QDs. Aliquots were taken for the core Zn–Cu–In–Se core QDs.

Synthesis of core/shell CIZSe/ZnS QDs

After the core synthesis, the shell solution consisting of precursors, $Zn(NO_3)_2 \cdot 6H_2O$ (1.68 mmol), *N*-acetyl-L-cysteine (2.58 mmol) and thiourea CH_4N_2S (4.38 mmol) in 10 mL of Milli-Q water at pH 6 was simultaneously added dropwise to the microwave reactor which was further subjected to microwave heating at 180 W for 2 min to form core/shell Zn–Cu–In–Se/ZnS QDs. Aliquots were taken and the resulting QDs were subjected to dialysis to purify and remove unwanted impurities. Followed by precipitation of synthesized QDs with propan-2-ol, centrifugation for 10 min at 8000 rpm, washing for three cycles and keeping the resultant QDs to dry under normal conditions. For the synthesis of Zn–Cu–In–Se core QDs with varying Zn : Cu molar ratios (from 0.0 to 5.0), the feed molar ratios of Zn and Cu precursors in core were varied with the total amount of Zn and Cu unaltered while keeping all the other reaction conditions the same.

Characterization

The morphology and structure of CIZSe/ZnS QDs were determined by transmission electron microscopy (TEM) on a JEOL ARM 200F cold FEG TEM/STEM equipped with a GIF quantum ER model 965, operating at 200 kV with a pixel resolution of 0.12 nm. High-angle annular dark-field scanning transmission electron microscopy (HAADF-STEM) and two-dimensional elemental mapping using energy-dispersive X-ray spectroscopy (EDX) were employed to determine the chemical composition of QDs.

Powder X-ray diffraction (XRD) patterns were obtained using Cu Kα radiation ($\lambda = 0.15418$ nm) on a Panalytical X'Pert Pro MPD diffractometer instrument.

X-ray photoelectron spectra (XPS) were recorded on a Gammadata Scienta SES 200-2 spectrometer. Inductively Coupled Plasma-Optical Emission Spectrometer (ICP-OES) measurements were conducted on a Varian 720-ES equipment.

Thermogravimetric analysis (TGA) was conducted under air from 20 to 800 °C at a heating rate of 10 °C min^{-1} using a TGA/DSC1 STAR equipment (Mettler-Toledo).

Dynamic light scattering (DLS) experiments and zeta potential measurements were carried out on a Zetasizer Nano ZS at 20 °C in water (green laser beam 532 nm) with a disposable capillary cell (DTS1070) (Malvern-Panalytical, UK). All measurements were performed in triplicate.

The Fourier transform infrared (FT-IR) spectra were recorded on a Bruker ALPHA spectrometer. The UV-visible absorption spectra were recorded using a Thermo Scientific Evolution 220 spectrometer. UV-visible-near infrared diffuse reflectance spectra were recorded a Shimadzu 2600–2700 spectrometer. The PL measurements were conducted using a SAFAS Xenius spectrophotometer equipped with a Xenon lamp as the excitation source. PL spectra were spectrally corrected and PL QYs were determined relative to Rhodamine 6G in ethanol (PL QY = 94%).

For the time resolved photoluminescence (TR-PL) experiments, the QDs were pumped by the 355 nm line of a frequency-tripled YAG (yttrium aluminium garnet):Nd laser. The laser pulse frequency, energy and duration were typically equal to 10 Hz, 50 μJ and 10 ns, respectively. The PL signal was analysed by a monochromator equipped with a 600 grooves per mm grating and by a photomultiplier tube cooled at 190 K. The rise time of the detector is equal to around 3 ns.

Mott–Schottky plots at 1–10 kHz frequencies were determined from EIS measurements in the dark, using 0.5 M Na_2SO_4 (pH = 7). The Mott–Schottky measurements are based on eqn (1):

$$\left(\frac{1}{C}\right)^2 = \frac{2}{(\varepsilon_r \varepsilon_0 A^2 e N_d)}\left(V - V_{fb} - \frac{k_B T}{e}\right) \quad (1)$$

where C is the space charge capacitance, e is the electronic charge, ε_r is the relative permittivity of materials, ε_0 is the permittivity of vacuum, N_d is the carrier concentration, k_B is the Boltzmann's constant, T is the absolute temperature, A is the area of electrode, V is the applied potential and V_{fb} is the flat-band potential (V_{FB}) that was determined by extrapolating the linear portion of the Mott–Schottky plot to V axis. The measured V_{FB} *vs.* Ag/AgCl were converted to the NHE scale using eqn (2):

$$V_{NHE} = V_{Ag/AgCl} + 0.197 \quad (2)$$

For Mott–Schottky measurements, the samples were prepared as follows. The 125 nm thick TiO_2 layer was deposited onto FTO substrates (fluorine doped tin oxide coated glass, TEC

7 Ω sq^{-1}) by DC magnetron sputtering of a pure Ti target (80 W for 15 min 48 s) and next annealed for 2 h at 500 °C. CIZSe/ZnS QDs were deposited onto FTO by dip-coating (20 cycles) from the purified stock solution. The deposited sample dried for 12 h under ambient conditions and then heated for 5 h at 300 °C under nitrogen.

Data availability

The data supporting this article have been included as part of the ESI.†

Author contributions

Thomas Gries and Raphaël Schneider supervised this study. Shubham Shishodia performed the synthesis and some characterization of QDs and photoelectro-measurements. Hervé Rinnert, Lavinia Balan, Jordane Jasniewski, Stéphanie Bruyère, and Ghouti Medjahdi performed the characterization of QDs. Shubham Shishodia, Thomas Gries, and Raphaël Schneider wrote the manuscript.

Conflicts of interest

There are no conflicts to declare.

Acknowledgements

This work was supported by the European Union's Horizon 2020 Research and Innovation Program under Grant Agreement 963530 and from the Agence Nationale de la Recherche ANR (project QDSOC).

Notes and references

1 D. Bera, L. Qian, T. K. Tseng and P. H. Holloway, *Materials*, 2010, **3**, 2260–2345.
2 M. Liu, N. Yazdani, M. Yarema, M. Jansen, V. Wood and E. H. Sargent, *Nat. Electron.*, 2021, **4**, 548–558.
3 X. Huang and M. Tang, *J. Appl. Toxicol.*, 2021, **41**, 342–361.
4 O. Yarema, M. Yarema and V. Wood, *Chem. Mater.*, 2018, **30**, 1446–1461.
5 T. Torimoto, T. Kameyama, T. Uematsu and S. Kuwabata, *J. Photochem. Photobiol., C*, 2023, **54**, 100569.
6 L. Yang, S. Zhang, B. Xu, J. Jiang, B. Cai, X. Lv, Y. Zou, Z. Fan, H. Yang and H. Zeng, *Nano Lett.*, 2023, **23**, 2443–2453.
7 S. Shishodia, B. Chouchene, T. Gries and R. Schneider, *Nanomaterials*, 2023, **13**, 2889.
8 L. Jin, G. S. Selopal, X. Tong, D. F. Perepichka, Z. M. Wang and F. Rosei, *Adv. Mater.*, 2024, 2402912.
9 L. Jin, J. Liu, X. Liu, D. Benetti, G. S. Selopal, X. Tong, E. Hamzehpoor, F. Li, D. F. Perepichka, Z. M. Wang and F. Rosei, *Small Methods*, 2024, **8**, 2300133.
10 M. Mrad, B. Chouchene, T. Ben Chaabane, T. Gries, G. Medjahdi, L. Balan and R. Schneider, *Catalysts*, 2022, **12**, 1585.
11 J. Du, R. Singh, I. Fedin, A. S. Fuhr and V. I. Klimov, *Nat. Energy*, 2020, **5**, 409–417.
12 L. J. Lim, X. Zhao and Z. K. Tan, *Adv. Mater.*, 2023, **35**, 2301887.
13 Z. Guan, J. Pan, Q. Li, G. Li and J. Yang, *ACS Sustainable Chem. Eng.*, 2019, **7**, 7736–7742.
14 C. F. Du, T. You, L. Jiang, S. Q. Yang, K. Zou, K. L. Han and W. Q. Deng, *RSC Adv.*, 2014, **4**, 33855–33860.
15 H. J. Yun, J. Lim, J. Roh, D. C. Jin Neo, M. Law and V. I. Klimov, *Nat. Commun.*, 2020, **11**, 5280.
16 J. Yang, J. Y. Kim, J. H. Yu, T. Y. Ahn, H. Lee, T. S. Choi, Y. W. Kim, J. Joo, M. J. Ko and T. Yyeon, *Phys. Chem. Chem. Phys.*, 2013, **15**, 20517–20525.
17 F. Liu, J. Zhu, Y. Xu, L. Zhou and S. Dai, *Nanoscale*, 2016, **8**, 10021–10025.
18 X. Tong, Y. Zhou, L. Jin, K. Basu, R. Adhikari, G. S. Selopal, X. Tong, H. Zhao, S. Sun, A. Vomiero, Z. M. Wang and F. Rosei, *Nano Energy*, 2017, **31**, 441–449.
19 F. E. S. Gorris, M. Deffner, S. Priyadarshi, C. Klinke, H. Weller and H. Lange, *Adv. Opt. Mater.*, 2020, **8**, 1901058.
20 I. Mehmood, Y. Liu, K. Chen, A. H. Shah and W. Chen, *RSC Adv.*, 2017, **7**, 33106–33112.
21 S. M. Harvey, D. W. Houck, W. Liu, Y. Liu, D. J. Gosztola, B. A. Korgel, M. R. Wasielewski and R. D. Schaller, *ACS Nano*, 2021, **15**, 19588–19599.
22 H. Zhong, Z. Wang, E. Bovero, Z. Lu, F. C. J. M. van Veggel and G. D. Scholes, *J. Phys. Chem. C*, 2011, **115**, 12396–12402.
23 H. McDaniel, N. Fuke, J. M. Pietryga and V. I. Klimov, *J. Phys. Chem. Lett.*, 2013, **4**, 355–361.
24 M. G. Panthani, C. J. Stolle, D. K. Reid, D. J. Rhee, T. B. Harvey, V. A. Akhavan, Y. Yu and B. A. Korgel, *J. Phys. Chem. Lett.*, 2013, **4**, 2030–2034.
25 B. K. Graeser, C. J. Hages, W. C. Yang, N. J. Carter, C. K. Miskin, E. A. Stach and R. Agrawal, *Chem. Mater.*, 2014, **26**, 4060–4063.
26 W. Li, Z. Pan and X. Zhong, *J. Mater. Chem. A*, 2015, **3**, 1649–1655.
27 J. Du, Z. Du, J. S. Hu, Z. Pan, Q. Shen, J. Sun, D. Long, H. Dong, L. Sun, X. Zhong and L. J. Wan, *J. Am. Chem. Soc.*, 2016, **138**, 4201–4216.
28 L. Zhang, Z. Pan, W. Wang, J. Du, Z. Ren, Q. Shen and X. Zhong, *J. Mater. Chem. A*, 2017, **5**, 21442–21451.
29 H. Song, Y. Lin, M. Zhou, H. Rao, Z. Pan and X. Zhong, *Angew. Chem., Int. Ed.*, 2021, **60**, 6137–6144.
30 R. Guo, J. Meng, W. Lin, A. Liu, T. Pullerits, K. Zheng and J. Tian, *J. Chem. Eng.*, 2021, **403**, 126452.
31 S. Yamashita, M. Tanabe, T. Araki, M. Shiomi, T. Nishi and Y. Kudo, *J. Phys. Chem. C*, 2022, **126**, 14558–14565.
32 B. Luo, J. Liu, H. Guo, X. Liu, R. Song, K. Shen, Z. M. Wang, D. Jing, G. S. Selopal and F. Rosei, *Nano Energy*, 2021, **88**, 106220.
33 W. Lian, D. Tu, X. Weng, K. Yang, F. Li, D. Huang, H. Zhu, Z. Xie and X. Chen, *Adv. Mater.*, 2024, **36**, 2311011.
34 M. A. Abate, K. Dehvari, J. Y. Chang and K. Waki, *Dalton Trans.*, 2019, **48**, 16115–16122.

35 Y. Jia, H. Liu, P. Cai, X. Liu, L. Wang, L. Ding, G. Xu, W. Wang, M. Jiao and X. Luo, *Chem. Commun.*, 2021, **57**, 4178–4181.
36 H. Liu, P. Cai, K. J. McHugh, C. F. Perkinson, L. Li, S. Wang, W. Wang, M. Jiao, X. Luo and L. Jing, *Nano Res.*, 2022, **15**, 8351–8359.
37 N. Irmania, K. Dehvari and J. Y. Chang, *J. Biomater. Appl.*, 2022, **36**, 1617–1628.
38 X. Kang, Y. Yang, L. Huang, Y. Tao, L. Wang and D. Pan, *Green Chem.*, 2015, **17**, 4482–4488.
39 S. Qu, X. Yuan, Y. Li, X. Li, X. Zhou, X. Xue, K. Zhang, J. Xu and C. Yuan, *Nanoscale Adv.*, 2021, **3**, 2334–2342.
40 P. Priyadarshini, S. Senapati, S. Bisoyi, S. Samal and R. Naik, *J. Alloys Compd.*, 2023, **945**, 169222.
41 P. Galiyeva, H. Rinnert, L. Balan, H. Alem, G. Medjahdi, B. Uralbekov and R. Schneider, *Appl. Surf. Sci.*, 2021, **562**, 150143.
42 P. Galiyeva, H. Alem, H. Rinnert, L. Balan, S. Blanchard, G. Medjahdi, B. Uralbekov and R. Schneider, *Inorg. Chem. Front.*, 2019, **6**, 1422–1431.
43 M. Mrad, T. Ben Chaabane, H. Rinnert, L. Balan, J. Jasniewski, G. Medjahdi and R. Schneider, *Inorg. Chem.*, 2020, **59**, 6220–6231.
44 H. McDaniel, N. Fuke, J. M. Pietryga and V. I. Klimov, *J. Phys. Chem. Lett.*, 2013, **4**, 355–361.
45 J. Ning, Y. Xiong, F. Huang, Z. Duan, S. V. Kershaw and A. L. Rogach, *Chem. Mater.*, 2020, **32**, 7842–7849.
46 A. Radchanka, V. Hrybouskaya, A. Iodchik, A. W. Achtstein and M. Artemyev, *J. Phys. Chem. Lett.*, 2022, **13**, 4912–4917.
47 B. Shakeri and R. W. Meulenberg, *Langmuir*, 2015, **31**, 13433–13440.
48 W. Yue, S. Han, R. Peng, W. Shen, H. Geng, F. Wu, S. Taoe and M. Wang, *J. Mater. Chem.*, 2010, **20**, 7570–7578.
49 Y. Matsumoto, M. Omae, I. Watanabe and E. Sato, *J. Electrochem. Soc.*, 1986, **133**, 711–716.
50 Q. Li, T. Zhang, D. Cui and F. Li, *Dalton Trans.*, 2024, **53**, 7742–7750.
51 S. M. Kobosko, D. H. Jara and P. V. Kamat, *ACS Appl. Mater. Interfaces*, 2017, **9**, 33379–33388.
52 S. U. Rahayu, Y. R. Wang, J. B. Shi and M. W. Le, *Sustain. Energy Fuels*, 2024, **8**, 113–124.